Validation of GOCE Models in Africa

Hussein A. Abd-Elmotaal

Civil Engineering Department, Faculty of Engineering
Minia University, Minia 61111, Egypt
abdelmotaal@lycos.com

Abstract

In modern geodesy, the geoid computation is carried out using the so-called remove-restore technique. In this technique, the effect of the topography and its isostatic compensation as well as the effect of a global reference field are removed from the gravimetric quantities being used in the geoid computation. The quality of the reference geopotential model used in the framework of the remove-restore technique plays a great role in estimating the accuracy of the computed geoid. In the last decade, the GOCE gravity field dedicated satellite mission has taken place in order to enhance the gravity field recovery worldwide. Numerous GOCE geopotential models have already been released. Each geopotential model depends on the strategy of the solution and the inclusion of terrestrial gravity data. The main aim of this paper is to validate the recently released GOCE geopotential models in Africa. The results show that the EIGEN-6C4 and GO_CONS_GCF_2_DIR_R5 models give the smallest standard deviation and range of the reduced isostatic anomalies, respectively. However, the range and the standard deviation of the reduced isostatic anomalies are relatively too high, which shows that none of the GOCE released geopotential models ideally fits the African gravity field.

Keywords: Harmonic synthesis, geopotential models, Africa, gravity anomaly.

1. Introduction

The global geopotential models are widely used in practice in many geodetic applications, such as gravity reduction, gravity smoothing, gravity interpolation and geoid computation. In the frame of the remove-restore geoid determination technique, the global geopotential models play an important role by introducing the effect of the long wavelength component of the gravity field. Hence, the proper choice of a global geopotential model in a geodetic application depends on how such a geopotential model fits the gravity field of the area of interest. The main aim of the current investigation is to examine how suitable the recently released GOCE global geopotential models are to the geodetic applications in Africa.

A number of recently available GOCE global geopotential models are considered for the current study. The local point free-air gravity anomaly data set for Africa is illustrated along with the available Digital Height Models necessary for the gravity reduction computations. The used formulas to compute the synthesized gravity anomalies from high-degree geopotential models are given. The used window remove-restore technique (Abd-Elmotaal and Kühtreiber, 2003) is outlined. The synthesized free-air gravity anomalies for Africa using the newly released GOCE global geopotential models are computed. The isostatic reduced gravity anomalies for Africa using the newly released GOCE global geopotential models are computed and widely discussed.

2. Used Geopotential Models

Table 1 illustrates the recently released GOCE global geopotential models used in the current investigation. For the sake of completeness, the EGM2008 global geopotential model is also used. Table 1 shows the models, their available maximum degree as well as the data used to develop these models. The following abbreviations are adopted for the used type of data in developing the geopotential models:

S = Satellite Tracking Data
G = Gravity Data
A = Altimetry Data

A wide range of geopotential models from satellite-only models with low maximum degree to combined models with ultra high-degree are considered for the current study.

Table 1: Used global geopotential models

Model	Year	Degree	Used Data	Reference
EGM2008	2008	2160	S(Grace),G,A	Pavlis et al., 2008, 2012
EIGEN-6C2	2012	1949	S(Goce,Grace,Lageos),G,A	Förste et al., 2012
EIGEN-6C4	2014	2190	S(Goce,Grace,Lageos),G,A	Förste et al., 2014
GO_CONS_GCF_2_TIM_R3	2011	250	S(Goce)	Pail et al., 2011
GO_CONS_GCF_2_TIM_R5	2014	280	S(Goce)	Brockmann et al., 2014
GO_CONS_GCF_2_DIR_R5	2014	300	S(Goce,Grace,Lageos)	Bruinsma et al., 2014
GOGRA02S	2013	230	S(Goce,Grace)	Yi et al., 2013
GOGRA04S	2014	230	S(Goce,Grace)	Yi et al., 2013
JYY_GOCE04	2014	230	S(Goce)	Yi et al., 2013
ITG-GOCE02	2013	240	S(Goce)	Schall et al., 2014

3. The Data

3.1. Point Free-Air Gravity Anomalies

All currently available sea and land point free-air gravity anomalies for Africa are used in the current investigation. Figure 1 shows their distribution. The distribution of the point free-air gravity anomaly stations on land is very poor. Many areas are empty. The distribution of the data points on sea is much better. More detailed information about the free-air data for Africa, the technique used for the needed gross-error detection and the merging technique can be found in (Abd-Elmotaal et al., 2015).

A total number of 1,186,032 free-air gravity anomaly values are available (cf. Fig. 1). The point free-air gravity anomalies range between −409.67 mgal and 452.80 mgal with an average of −4.37 mgal and a standard deviation of about 39.61 mgal.

In order to plot the free-air anomalies, they have been gridded on a $5' \times 5'$ grid using Kriging interpolation technique. Figure 2 shows the gridded $5' \times 5'$ free-air gravity anomalies for Africa used for the current investigation.

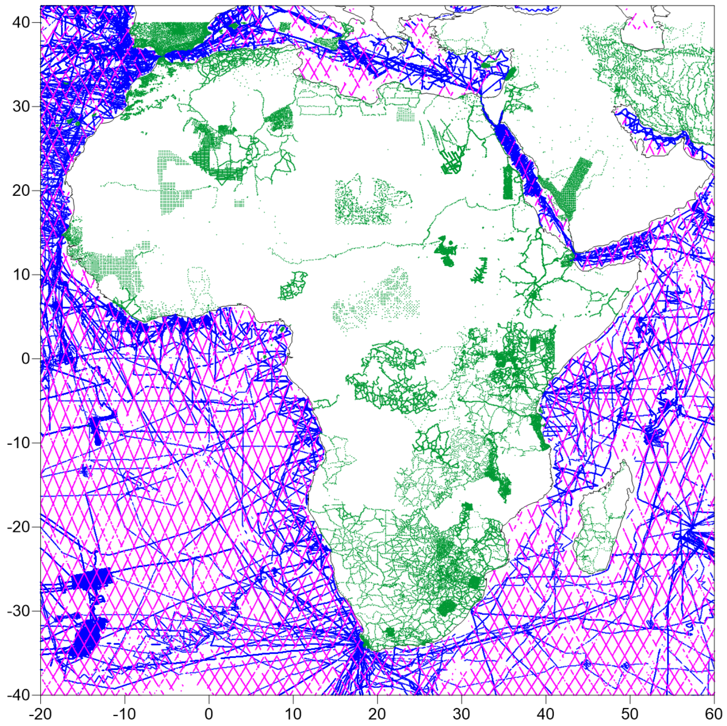

Figure 1: Distribution of the point free-air land (green), shipborne (blue) and altimetry derived (magenta) gravity anomalies in Africa.

3.2. Digital Height Models

For the terrain reduction computation, a set of fine and coarse Digital Height Models (DHM's) is needed. The $30'' \times 30''$ SRTM30+ (Farr et al., 2007), which includes topography and bathymetry, is employed as fine DHM, and the $3' \times 3'$ SRTM is used as coarse DHM. Figure 3 illustrates the $30'' \times 30''$ SRTM30+ fine DHM.

4. Basic Equations

The gravitational potential V can be expressed in spherical harmonic expansion as (Torge, 1989, p. 28; Dragomir et al., 1982, p. 53)

$$V(r,\theta,\lambda) = \frac{GM}{r}\left[1 + \sum_{n=2}^{\infty}\left(\frac{a}{r}\right)^n \sum_{m=0}^{n}\left(\bar{C}_{nm}\cos m\lambda + \bar{S}_{nm}\sin m\lambda\right)\bar{P}_{nm}(\cos\theta)\right], \quad (1)$$

where GM is the geocentric gravitational constant, r is the geocentric radius, θ is the polar distance, λ is the geodetic longitude, a stands for the equatorial radius of the mean earth's ellipsoid, $\bar{P}_{nm}$ denotes the associated fully normalized Legendre functions and $\bar{C}_{nm}$ and $\bar{S}_{nm}$ are the fully normalized potential coefficients. The polar distance θ can simply be expressed in terms of the geocentric latitude ψ as:

$$\theta = 90^{\circ} - \psi\,, \quad (2)$$

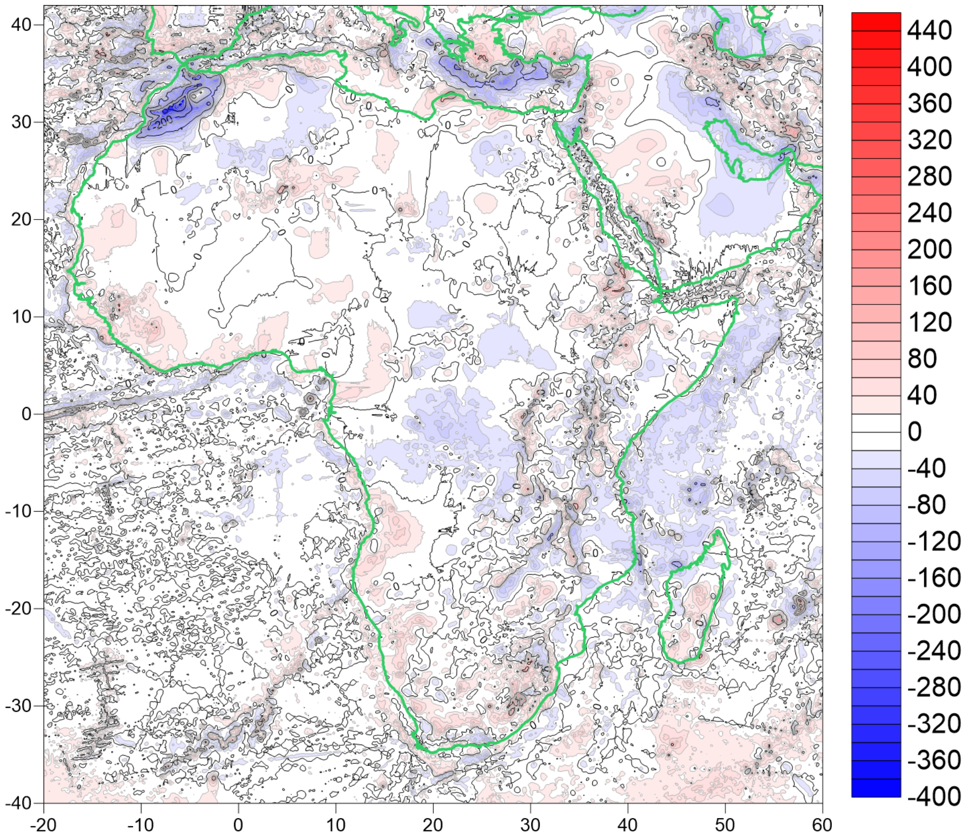

Figure 2: Gridded $5' \times 5'$ free-air gravity anomalies for Africa using the point gravity anomalies. Contour interval: 20 mgal.

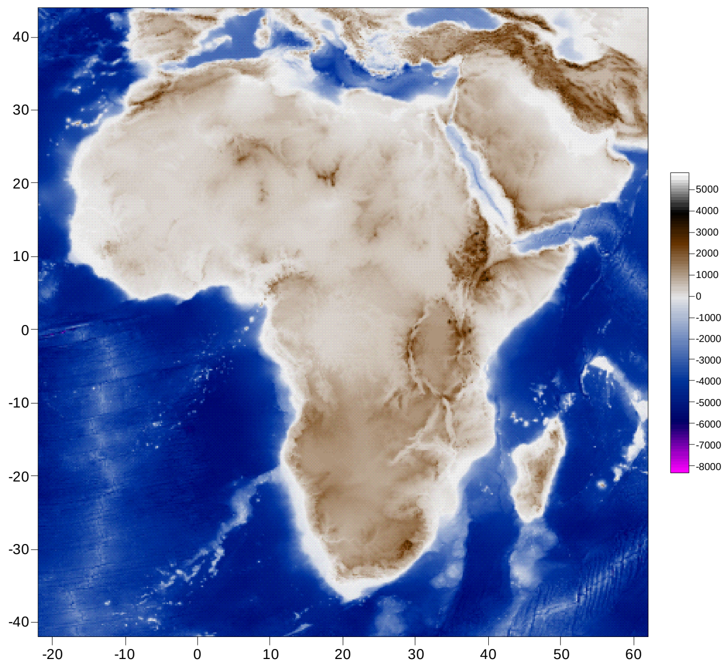

Figure 3: The fine $30'' \times 30''$ SRTM30+ DHM. Units in [m].

where ψ is related to the geodetic latitude ϕ through the following expression (Torge, 1980, p. 50):

$$\tan\psi = (1-f)^2 \tan\phi\,, \tag{3}$$

where f is the flattening of the earth's ellipsoid.

The disturbing potential T is defined by

$$T(r,\theta,\lambda) = V(r,\theta,\lambda) - U(r,\theta) \tag{4}$$

where U is the normal gravitational potential of the mean earth's ellipsoid, given by (Torge, 1989, p. 37)

$$U(r,\theta) = \frac{GM}{r}\left[1 + \sum_{n=2}^{\infty}\left(\frac{a}{r}\right)^n \bar{C}^u_{n0}\bar{P}_{n0}(\cos\theta)\right]. \tag{5}$$

Here $\bar{C}^u_{n0}$ denotes the fully normalized harmonic coefficients implied by the reference equipotential ellipsoid. Because of the rotational symmetry of the mean earth's ellipsoid, there will be only zonal terms. And because of the symmetry with respect to the equatorial plane, there will be only even zonal harmonics $\bar{C}^u_{2n,0}$ (Heiskanen and Moritz, 1967, p. 72). The even degree zonal harmonic coefficients $\bar{C}^u_{2n,0}$ converge quickly toward zero, so that (5) may safely be truncated after $n = 6$.

Thus inserting (1) and (5) into (4), the disturbing potential T can be expressed as (Torge, 1989, p. 43)

$$T(r,\theta,\lambda) = \frac{GM}{r}\sum_{n=2}^{\infty}\left(\frac{a}{r}\right)^n \sum_{m=0}^{n}\left(\bar{C}^*_{nm}\cos m\lambda + \bar{S}_{nm}\sin m\lambda\right)\bar{P}_{nm}(\cos\theta)\,, \tag{6}$$

where $\bar{C}^*_{nm}$ is the difference between the actual coefficients $\bar{C}_{nm}$ and those implied by the reference equipotential ellipsoid $\bar{C}^u_{nm}$.

The gravity anomaly Δg can be expressed, using the spherical approximation, by (Moritz, 1980)

$$\Delta g(r,\theta,\lambda) = \frac{GM}{r^2}\sum_{n=2}^{\infty}(n-1)\left(\frac{a}{r}\right)^n \sum_{m=0}^{n}\left(\bar{C}^*_{nm}\cos m\lambda + \bar{S}_{nm}\sin m\lambda\right)\bar{P}_{nm}(\cos\theta)\,. \tag{7}$$

5. The Window Technique

The traditional way of removing the effect of the topographic-isostatic masses faces a theoretical problem. A part of the influence of the topographic-isostatic masses is removed twice as it is already included in the global reference field. This leads to some double consideration of that part of the topographic-isostatic masses. Figure 4 sketches the traditional gravity reduction for the effect of the topographic-isostatic masses. The short-wavelength part, depending on the topographic-isostatic masses, is computed for a point P for the masses inside the circle denoted by TC. Removing the effect of the long-wavelength part by a global earth's gravitational potential field normally implies removing the influence of the global topographic-isostatic masses, shown as the big rectangle in Fig. 4 denoted by EGM (here EGM stands for Global Geopotential Model).

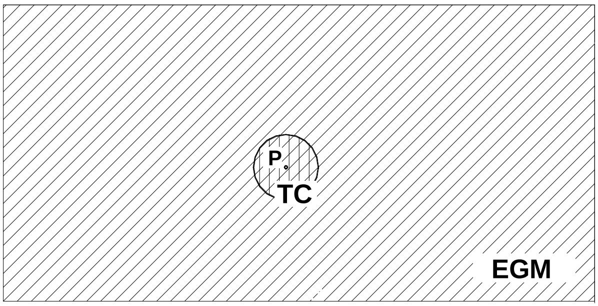

Figure 4: The traditional remove-restore technique.

The double consideration of the topographic-isostatic masses inside the circle (double hatched) is thus seen.

A possible way to overcome this difficulty is to adapt the used reference field to the effect of the topographic-isostatic masses for a fixed data area (Abd-Elmotaal and Kühtreiber, 2003). Figure 5 shows the advantage of the window remove-restore technique. Consider a measurement at point P; the short-wavelength part, depending on the topographic-isostatic masses, is now computed by using the masses of the whole data area (the small rectangle in Fig. 5). The adapted reference field is created by subtracting the effect of the topographic-isostatic masses of the data window, in terms of potential coefficients, from the reference field coefficients. Thus, removing the long-wavelength part by using this adapted reference field does not lead to a double consideration of a part of the topographic-isostatic masses (as there is no double hatched area in Fig. 5).

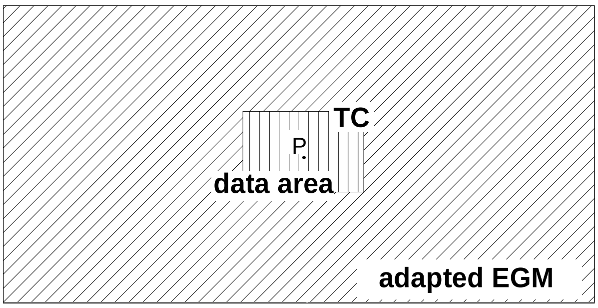

Figure 5: The window remove-restore technique.

The remove step of the window remove-restore technique can then mathematically be written as

$$\Delta g_{iso\,win} = \Delta g_F - \Delta g_{TI\,win} - \Delta g_{GM\,Adapt}\,, \tag{8}$$

where $\Delta g_{iso\,win}$ stands for the isostatic anomalies computed using the window technique, $\Delta g_{GM\,Adapt}$ is the contribution of the adapted reference field and $\Delta g_{TI\,win}$ is the effect of topography and its compensation for the fixed data window on the gravity anomalies employing the fine and coarse DHM's described in sec. 3.2.Equation (8) can be written more explicitly as

$$\begin{aligned}\Delta g_{iso\,win} &= \Delta g_F - \Delta g_{TI\,win} - (\Delta g_{GM} - \Delta g_{wincof}) \\ &= \Delta g_F - \Delta g_{TI\,win} - \Delta g_{GM} + \Delta g_{wincof}\,, \end{aligned} \tag{9}$$

where Δg_{GM} is the contribution of the original global reference field and Δg_{wincof} is the contribution of the harmonic coefficients of the topographic-isostatic masses of the data window (for our case it is the African data window $-40° \leq \phi \leq 42°$, $-20° \leq \lambda \leq 60°$) computed to the maximum degree of the used geopotential model.

The computation of the potential harmonic coefficients of the topographic-isostatic masses within the data window is carried out using (Abd-Elmotaal and Kühtreiber, 1999, Eq. (11)). The contribution Δg_{wincof} is computed from the potential harmonic coefficients of the topographic-isostatic masses within the data window (for our case it is the African data window). For more details on the window remove-restore technique, the reader is kindly invited to refer to (Abd-Elmotaal and Kühtreiber, 1999, 2003).

Let us define a couple of terms. The first term is called "the long-medium wavelength free-air anomalies" $\Delta g_{F\ long\text{-}med}$, which is defined as

$$\Delta g_{F\ long\text{-}med} = \Delta g_F - \Delta g_{TI\ win} + \Delta g_{wincof}\ . \tag{10}$$

The second term is called "the reduced free-air anomalies" $\Delta g_{F\ red}$, which is defined as

$$\Delta g_{F\ red} = \Delta g_F - \Delta g_{GM}\ . \tag{11}$$

6. The Results

Table 2 shows the statistics of the point free-air gravity anomalies as well as of the free-air anomalies produced by the used global geopotential models. The program GRVHRM (Abd-Elmotaal, 1998) has been used to compute the free-air gravity anomalies at the gravity data points produced by the used geopotential models Δg_{GM}.

Table 2: Statistics of the free-air gravity anomalies produced by the used global geopotential models (1,186,032 stations). Units in [mgal]

gravity anomalies	N_{max}	min.	max.	mean	st. dev.
Point free-air (Δg_F)	—	−409.67	452.80	−4.37	39.61
$\Delta g_{F\ long\text{-}med}$	—	−237.16	322.42	−3.28	36.30
EGM2008	2160	−234.72	578.21	−2.51	38.14
EIGEN-6C2	1949	−237.06	573.60	−2.52	37.97
EIGEN-6C4	2190	−233.70	579.57	−2.50	37.96
GO_CONS_GCF_2_TIM_R3	250	−191.72	176.16	−0.86	28.26
GO_CONS_GCF_2_TIM_R5	280	−185.04	190.75	−0.96	29.11
GO_CONS_GCF_2_DIR_R5	300	−182.12	190.64	−1.02	29.35
GOGRA02S	230	−197.34	176.59	−0.93	28.27
GOGRA04S	230	−196.16	176.96	−0.81	28.24
JYY_GOCE04S	230	−196.06	176.90	−0.81	28.24
ITG-GOCE02	240	−190.47	175.88	−0.69	27.97

According to Eq. (9), in order to get as much smaller reduced anomalies as possible, the term "the long-medium wavelength free-air anomalies" $\Delta g_{F\ long\text{-}med}$ should compensate with the term Δg_{GM}. Accordingly, Table 2 may give the sign that none of the examined geopotential models would satisfy this criterion. The range of the long-medium wavelength free-air anomalies $\Delta g_{F\ long\text{-}med}$ is only 65% of that of the free-air anomalies and the standard deviation is about 92% of that of the free-air anomalies (which signalizes that the short wavelength are mostly removed from the free-air anomalies). Table 2 shows that the ultra high-degree models have generally greater range than that of the long-medium wavelength free-air anomalies $\Delta g_{F\ long\text{-}med}$ with slightly higher standard deviation. In contradictory, the satellite-only models (which have low upper maximum degree) have generally much smaller range than that of the long-medium wavelength free-air anomalies $\Delta g_{F\ long\text{-}med}$ with significantly smaller standard deviation.

Table 3 shows the statistics of "the reduced free-air anomalies" $\Delta g_{F\ red}$ for all used global geopotential models. No topographic-isostatic reduction has been made at this stage. Table 3 shows that the range of the reduced free-air gravity anomalies $\Delta g_{F\ red}$ for all models is at the same order of magnitude as that of the point free-air gravity anomalies. It shows also that the standard deviation of the reduced free-air anomalies $\Delta g_{F\ red}$ for the ultra high-degree models is dramatically smaller than that of the satellite-only models. This is simply because the satellite-only models could not remove the medium wavelength from the free-air anomalies having a relatively low upper maximum degree. This may also come from the possible inclusion of some of the gravity measurements over Africa in the creation of the ultra-high geopotential models. Table 3 also shows that the mean value of the reduced free-air anomalies $\Delta g_{F\ red}$ for the ultra high-degree models is smaller than that of the satellite-only models.

Table 3: Statistics of the reduced free-air gravity anomalies $\Delta g_{F\ red}$ computed by Eq. (11) for the used global geopotential models (1,186,032 stations). Units in [mgal]

used geopotential model	N_{max}	min.	max.	mean	st. dev.
EGM2008	2160	−457.03	271.53	−1.86	13.24
EIGEN-6C2	1949	−473.32	272.07	−1.85	13.47
EIGEN-6C4	2190	−456.51	270.80	−1.88	13.35
GO_CONS_GCF_2_TIM_R3	250	−525.32	313.08	−3.51	29.10
GO_CONS_GCF_2_TIM_R5	280	−527.16	294.74	−3.41	27.94
GO_CONS_GCF_2_DIR_R5	300	−525.37	295.34	−3.35	27.68
GOGRA02S	230	−515.18	323.29	−3.44	29.22
GOGRA04S	230	−510.40	320.69	−3.56	29.09
JYY_GOCE04S	230	−510.44	320.57	−3.56	29.09
ITG-GOCE02	240	−518.39	316.61	−3.68	29.41

Figure 6 shows the free-air reduced gravity anomalies $\Delta g_{F\ red}$ for the EIGEN-6C4 geopotential model, being one of the best models to generate the reduced free-air anomalies for Africa. It should be noted that EGM2008 model gives nearly the same statistics of the reduced free-air gravity anomalies. Figure 6 shows that most of the area has free-air reduced gravity anomalies less than 20 mgal in magnitude (the white pattern). More than 91.4% of the points have reduced free-air anomalies less than 20 mgal in magnitude. The higher values are located at the high mountainous area of Morocco, which is likely due to vertical datum inconsistency. Deeper investigation for this area is essentially needed (cf. Abd-Elmotaal et al., 2015).

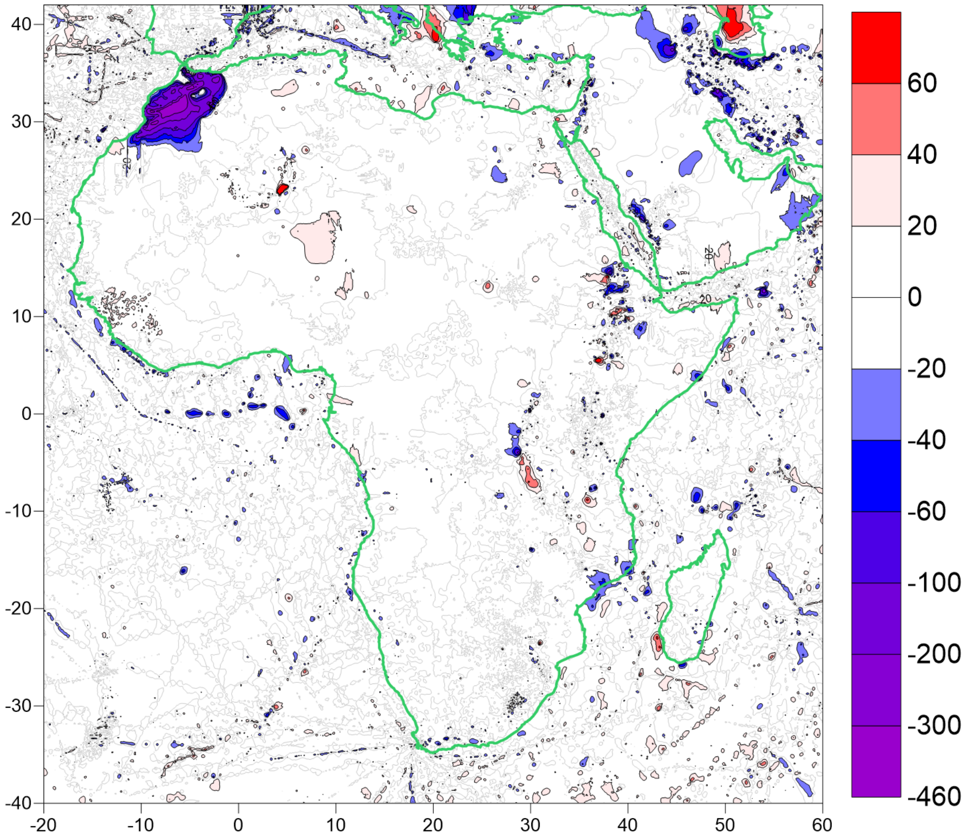

Figure 6: The EIGEN-6C4 reduced free-air anomalies $\Delta g_{F\,red}$ for Africa (computed by Eq. (11)).

Table 4 shows the statistics of the isostatic anomalies computed using the window technique $\Delta g_{iso\;win}$ for the used geopotential models. The Airy-Heiskanen isostatic model has been used with the following parameters:

$$\begin{aligned} T_\circ &= 30\ \text{km}\,, \\ \rho_\circ &= 2.67\ \text{g/cm}^3\,, \\ \Delta\rho &= 0.4\ \text{g/cm}^3\,. \end{aligned} \tag{12}$$

Table 4 shows that the standard deviation and the mean values of the Airy window isostatic gravity anomalies for the ultra high-degree models are slightly smaller than those of the satellite-only models. The range of the Airy window isostatic gravity anomalies for the ultra high-degree models is, however, significantly larger than that of the satellite-only models. Generally, the range and the standard deviation of the Airy window isostatic anomalies are relatively too high for such kind of gravity anomalies, which may signalize that none of these models is ideal for geodetic applications in Africa.

More interesting is the significant drop of the standard deviation of the the Airy window isostatic gravity anomalies for the satellite-only models. This already indicates an improvement, but perhaps not to the desired extent.

Table 4: Statistics of the isostatic anomalies computed using the window technique $\Delta g_{iso\,win}$ using Eq. (9) for the used global geopotential models (1,186,032 stations). Units in [mgal]

used geopotential model	N_{max}	min.	max.	mean	st. dev.
EGM2008	2160	−423.93	270.86	−0.77	20.09
EIGEN-6C2	1949	−409.02	271.40	−0.77	20.03
EIGEN-6C4	2190	−423.59	270.13	−0.79	20.00
GO_CONS_GCF_2_TIM_R3	250	−202.96	282.96	−2.42	22.86
GO_CONS_GCF_2_TIM_R5	280	−207.79	281.82	−2.33	21.55
GO_CONS_GCF_2_DIR_R5	300	−205.08	276.98	−2.26	21.22
GOGRA02S	230	−212.28	281.00	−2.35	23.10
GOGRA04S	230	−210.06	284.15	−2.47	23.02
JYY_GOCE04S	230	−209.96	284.10	−2.47	23.02
ITG-GOCE02	240	−207.72	285.43	−2.59	23.33

In order to distinguish between the case on land and on sea regions, two tables are established. Tables 5 and 6 show the statistics of the isostatic anomalies computed using the window technique $\Delta g_{iso\,win}$ for the used geopotential models on land and sea, respectively. Generally, the Airy window isostatic anomalies on land have slightly higher standard deviation and range than those on sea for all models.

Table 5: Statistics of the isostatic anomalies on land computed using the window technique $\Delta g_{iso\,win}$ using Eq. (9) for the used global geopotential models (94,838 stations). Units in [mgal]

used geopotential model	N_{max}	min.	max.	mean	st. dev.
EGM2008	2160	−423.93	270.86	−0.39	23.65
EIGEN-6C2	1949	−409.02	271.40	−0.34	23.59
EIGEN-6C4	2190	−423.59	270.13	−0.19	23.70
GO_CONS_GCF_2_TIM_R3	250	−202.96	282.96	−0.27	25.38
GO_CONS_GCF_2_TIM_R5	280	−207.79	281.82	−0.52	23.96
GO_CONS_GCF_2_DIR_R5	300	−205.08	276.98	−0.53	23.62
GOGRA02S	230	−212.28	281.00	−0.14	25.81
GOGRA04S	230	−210.06	284.15	−0.14	25.68
JYY_GOCE04S	230	−209.96	284.10	−0.14	25.68
ITG-GOCE02	240	−207.72	285.43	−0.16	25.77

Table 6: Statistics of the isostatic anomalies on sea computed using the window technique $\Delta g_{iso\,win}$ using Eq. (9) for the used global geopotential models (1,091,194 stations). Units in [mgal]

used geopotential model	N_{max}	min.	max.	mean	st. dev.
EGM2008	2160	−187.90	142.50	−0.81	19.75
EIGEN-6C2	1949	−186.05	145.02	−0.80	19.69
EIGEN-6C4	2190	−187.65	143.68	−0.84	19.65
GO_CONS_GCF_2_TIM_R3	250	−152.32	159.09	−2.61	22.62
GO_CONS_GCF_2_TIM_R5	280	−140.64	159.21	−2.48	21.32
GO_CONS_GCF_2_DIR_R5	300	−140.02	151.68	−2.41	21.00
GOGRA02S	230	−149.29	167.32	−2.55	22.84
GOGRA04S	230	−149.01	168.93	−2.67	22.76
JYY_GOCE04S	230	−149.08	168.99	−2.68	22.76
ITG-GOCE02	240	−153.41	170.45	−2.80	23.09

Figure 7 shows the Airy window isostatic gravity anomalies $\Delta g_{iso\,win}$ for the EIGEN-6C4 geopotential model, being the best model giving the smallest standard deviation of the Airy window isostatic anomalies. Figure 7 shows that most of the area has Airy window isostatic gravity anomalies less than 20 mgal in magnitude (the white pattern). More than 78.5% of the points have Airy window isostatic anomalies less than 20 mgal in magnitude.

Figure 8 shows the Airy window isostatic gravity anomalies $\Delta g_{iso\,win}$ for the satellite-only GO_CONS_GCF_2_DIR_R5 geopotential model, which have a significantly better range than that of EIGEN-6C4 model (more than 210 mgal less) and a slightly larger standard deviation (1.2 mgal higher). The advantage of the GO_CONS_GCF_2_DIR_R5 geopotential model is that its upper maximum degree is only 300, which saves a tremendous amount of CPU time for computing the synthesized gravity anomalies Δg_{GM}. Figure 8 shows that most of the area has Airy window isostatic gravity anomalies less than 20 mgal in magnitude (the white pattern). More than 75.2% of the points have Airy window isostatic anomalies less than 20 mgal in magnitude.

7. Conclusion

Different recent GOCE geopotential models are tested to produce reduced isostatic gravity anomalies for Africa. The reduction of the gravity anomalies follows the window remove-restore technique employing the Airy floating hypothesis. A wide range of geopotential models are tested from satellite-only models, having low upper degree, to combined models having ultra high upper degree.

The results show that the GOCE-GRACE-LAGEOS combined geopotential model EIGEN-6C4 gives the smallest standard deviation of the Airy window isostatic anomalies for Africa. The GOCE satellite-only model GO_CONS_GCF_2_DIR_R5 gives the smallest range of the Airy window isostatic anomalies for Africa, with only 1 mgal higher in the

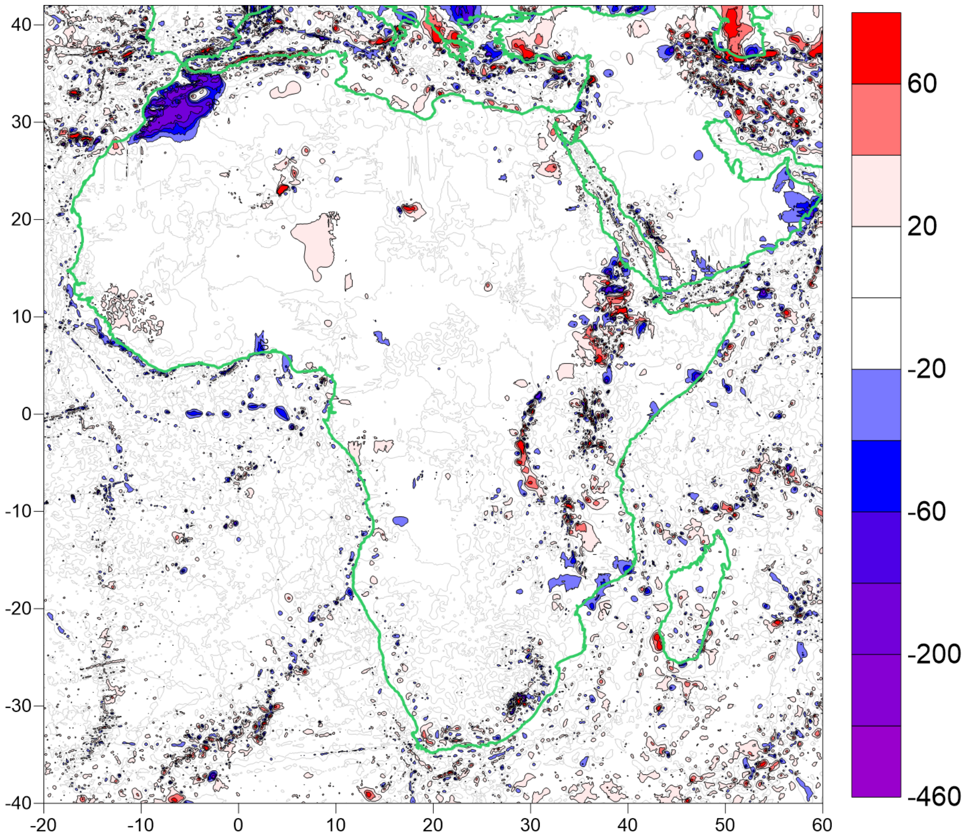

Figure 7: The EIGEN-6C4 Airy window isostatic anomalies $\Delta g_{iso\ win}$ for Africa (computed by Eq. (9)).

standard deviation compared to that of the EIGEN-6C4 model. Both the range and standard deviation of the Airy window isostatic anomalies generated by all tested models are relatively high.

It has been shown that most of the points on land in Africa have Airy window isostatic anomalies below 20 mgal in magnitude. There are still some spots, like in the high mountainous area of Morocco, that they still have large values of the Airy window isostatic anomalies. This needs, however, a deeper investigation. We believe that using some of the African land gravity measurement in the scaling process of the satellite-only models would definitely increase their fit to the African gravity field.

References

Abd-Elmotaal, H. (1998) An Alternative Capable Technique for the Evaluation of Geopotential from Spherical Harmonic Expansions, *Bollettino di Geodesia e Scienze Affini*, **57**, 25–38.

Abd-Elmotaal, H. and Kühtreiber, N. (1999) Improving the Geoid Accuracy by Adapting the Reference Field. *Physics and Chemistry of the Earth*, **24** (1), 53–59, DOI: 10.1016/S1464-1895(98)00010-6.

Abd-Elmotaal, H. and Kühtreiber, N. (2003) Geoid Determination Using Adapted Refer-

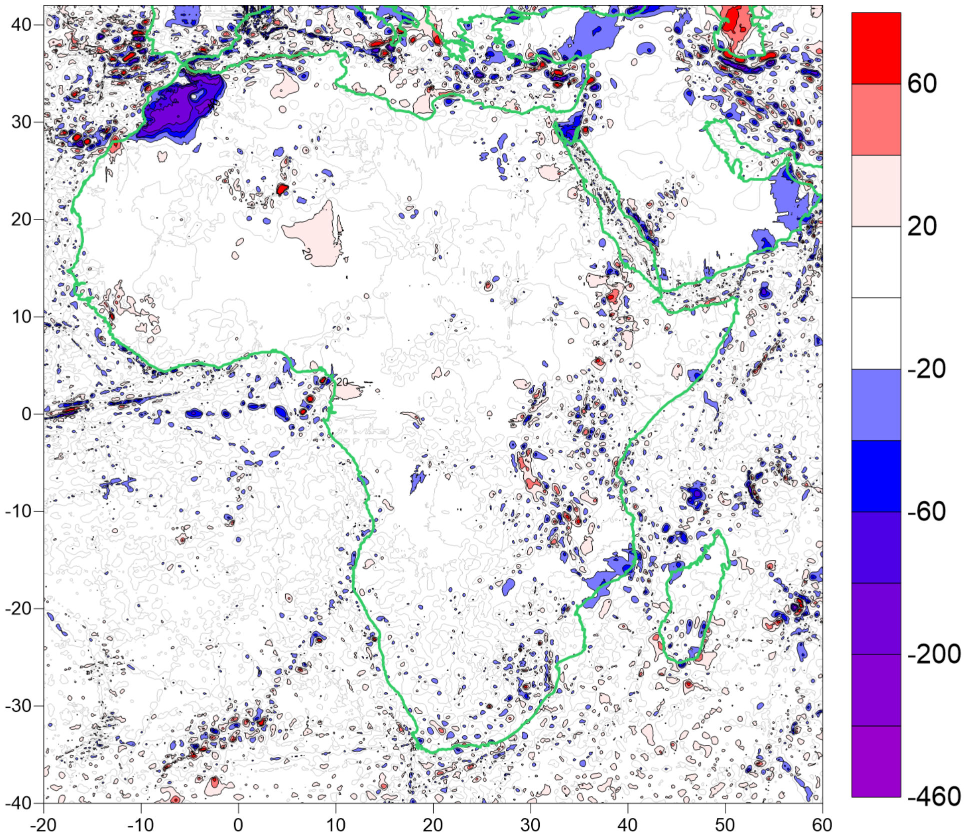

Figure 8: The GO_CONS_GCF_2_DIR_R5 Airy window isostatic anomalies $\Delta g_{iso\ win}$ for Africa (computed by Eq. (9)).

ence Field, Seismic Moho Depths and Variable Density Contrast, *Journal of Geodesy*, **77**, 77–85.

Abd-Elmotaal, H., Seitz, K, Kühtreiber, N. and Heck, B. (2015) Establishment of the Gravity Database for the African Geoid. *International Association of Geodesy Symposia Journal*, **144**, DOI: 10.1007/1345_2015_51.

Brockmann, J.M., Zehentner, N., Höck, E., Pail, R., Loth, I., Mayer-Gürr, T., and Schuh, W.-D. (2014) EGM_TIM_RL05: An independent geoid with centimeter accuracy purely based on the GOCE mission. *Geophysical Research Letters*, **41** (22), 8089–8099, DOI: 10.1002/2014GL061904.

Bruinsma, S.L., Förste, C., Abrikosov, O., Lemoine, J.-M., Marty, J.C., Mulet, S., Rio, M.H. and Bonvalot, S. (2014) ESA's Satellite-Only Gravity Field Model via the Direct Approach Based on all GOCE data. *Geophysical Research Letter*, **41** (21), 7508-7514, DOI: 10.1002/2014GL062045.

Dragomir, V.C., Ghiţău, D.N., Mikăilescu, M.S. and Rotaru, M.G. (1982) *Theory of the Earth's Shape: Developments in Solid Earth Geophysics, 13.* Elsevier Scientific Publishing Company, Amsterdam, Oxford, New York.

Farr, T.G., Rosen, P.A., Caro, E., Crippen, R., Duren, R., Hensley, S., Kobrick, M., Paller, M., Rodriguez, E., Roth, L., Seal, D., Shaffer, S., Shimada, J., Umland, J., Werner, M., Oskin, M., Burbank, D. and Alsdorf, D. (2007) The Shuttle Radar Topography Mission, *Reviews of Geophysics*, **45**, RG2004, DOI:10.1029/2005RG000183.

Förste, C., Bruinsma, S.L., Flechtner, F., Marty, J.-C., Lemoine, J.-M., Dahle, C., Abrikosov, O., Neumayer, H., Biancale, R., Barthelmes, F. and Balmino, G. (2012) A New Release of EIGEN-6C. *American Geophysical Union, Fall Meeting, San Francisco, USA, December 3–7, 2012.*

Förste C., Bruinsma, S.L., Abrikosov, O., Lemoine, J.-M., Schaller, T., Götze, H.-J., Ebbing, J., Marty, J.C., Flechtner, F., Balmino, G., Biancale, R. (2014) EIGEN-6C4 The Latest Combined Global Gravity Field Model Including GOCE Data Up to Degree and Order 2190 of GFZ Potsdam and GRGS Toulouse. *5th GOCE User Workshop, Paris, November 25–28, 2014.*

Heiskanen, W.A., and Moritz, H. (1967) *Physical Geodesy.* Freeman, San Francisco.

Moritz, H. (1980) *Advanced Physical Geodesy.* Wichmann, Karlsruhe.

Pail, R., Bruinsma, S., Migliaccio, F., Förste, C., Goiginger, H., Schuh, W.-D., Höck, E., Reguzzoni, M., Brockmann, J.M., Abrikosov, O., Veicherts, M., Fecher, T., Mayrhofer, R., Krasbutter, I., Sansò, F. and Tscherning, C.C. (2011) First GOCE Gravity Field Models Derived by Three Different Approaches. *Journal of Geodesy,* **85** (11), 819–843, DOI: 10.1007/s00190-011-0467-x.

Pavlis, N.K., Factor, J.K., Holmes, S.A. (2007) Terrain-Related Gravimetric Quantities Computed for the Next EGM, *Harita Dergisi; Özel Sayı: Gravity Field of the Earth, Proceedings of the 1st International Symposium of the International Gravity Field Service (IGFS), 28 August – 1 September, 2006, Istanbul, Turkey*, **18**, 318–323.

Pavlis, N.K., Holmes, S.A., Kenyon, S.C., and Factor, J.K. (2008) An Earth Gravitational Model to Degree 2160: EGM2008, *General Assembly of the European Geosciences Union, Vienna, Austria, April 13–18, 2008.*

Pavlis, N.K., Holmes, S.A., Kenyon, S.C., and Factor, J.K. (2012) The development and evaluation of the Earth Gravitational Model 2008 (EGM2008). *Journal of Geophysical Research* **117**, B04406, doi:10.1029/2011JB008916.

Schall J., Eicker, A., Kusche, J. (2014) The ITG-GOCE02 Gravity Field Model from GOCE Orbit and Gradiometer Data Based on the Short Arc Approach. *Journal of Geodesy*, **88**, 403–409, DOI: 10.1007/s00190-014-0691-2.

Torge, W. (1980) *Geodesy.* Walter de Gruyter, Berlin, New York.

Torge, W. (1989) *Gravimetry.* Walter de Gruyter, Berlin, New York.

Yi, W., Rummel, R., Gruber, T. (2013) Gravity Field Contribution Analysis of GOCE Gravitational Gradient Components. *Studia Geophysica et Geodaetica*, **57** (2), 174–202, DOI: 10.1007/s11200-011-1178-8.